Received: 22 January 2023 | Revised: 10 May 2023 | Accepted: 16 May 2023

DOI: 10.1002/glia.24392

GLIA

WILEY

RESEARCH ARTICLE

Spontaneous and multifaceted ATP release from astrocytes at the scale of hundreds of synapses

Yoshiki Hatashita[1] | Zhaofa Wu[2] | Hirotaka Fujita[1] | Takuma Kumamoto[3] | Jean Livet[3] | Yulong Li[2] | Manabu Tanifuji[1] | Takafumi Inoue[1]

[1]Department of Life Science and Medical Bioscience, Faculty of Science and Engineering, Waseda University, Tokyo, Japan

[2]School of Life Science, Peking University, Beijing, China

[3]Sorbonne Université, INSERM, CNRS, Institut de la Vision, Paris, France

Correspondence
Takafumi Inoue, Department of Life Science and Medical Bioscience, Faculty of Science and Engineering, Waseda University, Tokyo 162-8480, Japan.
Email: inoue.t@waseda.jp

Funding information
IHU FOReSIGHT, Grant/Award Number: ANR-18-IAHU-01; Postdoctoral Fellowship of Peking-Tsinghua Center for Life Scences; Waseda University, Grant/Award Numbers: 2019C-715, 2020C-778, 2021C-733, 2022C-629; Yoshida Scholarship Foundation, Grant/Award Number: Doctor 21

Abstract

Astrocytes participate in information processing by releasing neuroactive substances termed gliotransmitters, including ATP. Individual astrocytes come into contact with thousands of synapses with their ramified structure, but the spatiotemporal dynamics of ATP gliotransmission remains unclear, especially in physiological brain tissue. Using a genetically encoded fluorescent sensor, $GRAB_{ATP1.0}$, we discovered that extracellular ATP increased locally and transiently in absence of stimuli in neuron–glia co-cultures, cortical slices, and the anesthetized mouse brain. Spontaneous ATP release events were tetrodotoxin-insensitive but suppressed by gliotoxin, fluorocitrate, and typically spread over 50–250 μm^2 area at concentrations capable of activating purinergic receptors. Besides, most ATP events did not coincide with Ca^{2+} transients, and intracellular Ca^{2+} buffering with BAPTA-AM did not affect ATP event frequency. Clustering analysis revealed that these events followed multiple distinct kinetics, and blockade of exocytosis only decreased a minor group of slow events. Overall, astrocytes spontaneously release ATP through multiple mechanisms, mainly in non-vesicular and Ca^{2+}-independent manners, thus potentially regulating hundreds of synapses all together.

KEYWORDS
astrocytes, neuron–glia interactions, calcium imaging, extracellular ATP imaging, gliotransmission, exocytosis, channel-mediated ATP release

1 | INTRODUCTION

Astrocytes, the most abundant glial cells in the central nervous system, directly modulate synaptic activity and neuronal network dynamics by releasing neuroactive substances termed gliotransmitters (Araque et al., 2014; Halassa & Haydon, 2010). Gliotransmission is postulated as a feedback response to neuronal activity (Henneberger et al., 2010; Panatier et al., 2011; Perea & Araque, 2007). Astrocytes can discriminate inputs from different synaptic terminals (Perea, 2005) and utilize different gliotransmitters depending on the neuron firing frequency (Covelo & Araque, 2018). These notions suggest that they can interpret surrounding neuronal activity and provide relevant feedback control. Thus, astrocytes are now regarded as partners of neurons in information processing, whereas they were classically considered to play only supportive roles in the brain.

ATP is one of the major gliotransmitters and is considered essential for brain function because impaired astrocytic ATP release leads to deficiency in synaptic plasticity (Jun et al., 2018), depressive-like behavior (Cao et al., 2013; Jun et al., 2018; Wang et al., 2021), and sleep loss in rodents (Halassa et al., 2009). Not only is ATP released from astrocytes in response to neuronal inputs, but Koizumi et al. found tetrodotoxin-insensitive ATP release in neuron–glia co-culture (Koizumi et al., 2003). Tonic ATP release was reported in brain slice preparations (Chever et al., 2014; Chi et al., 2022; Kamatsuka et al., 2014), but it was unclear whether

astrocytes release ATP spontaneously or in response to the basal neuronal firing. Investigating basal ATP release activity will provide a further perspective on how astrocytes are involved in neuron network function.

Intracellular Ca^{2+} elevation in astrocytes has been implicated in ATP gliotransmission and can be triggered by various inputs including neurotransmitters, neuromodulators, changes in temperature, pH, and pressure, or even without stimulation (Guerra-Gomes et al., 2018; Semyanov, 2019; Shigetomi et al., 2016). Several groups have demonstrated that optogenetically or chemogenetically evoked Ca^{2+} increase in astrocytes leads to ATP release (Iwai et al., 2021; Mederos et al., 2019; Shen et al., 2017; Wang et al., 2021). Furthermore, spatiotemporally complex spontaneous Ca^{2+} elevations in astrocytes have been revealed (Agarwal et al., 2017; Bindocci et al., 2017; Haustein et al., 2014; Rungta et al., 2016; Takata & Hirase, 2008; Wu et al., 2019), with varied areas ranging from sub-micrometer order touching a single synapse (Arizono et al., 2020) to ones covering tens to thousands of synapses (Semyanov, 2019). Although the Ca^{2+}-dependent gliotransmission has been the subject of debate (Agulhon et al., 2012; Bazargani & Attwell, 2016; Fiacco & McCarthy, 2018; Savtchouk & Volterra, 2018), the above lines of evidence have prompted speculation that astrocytes locally regulate multiple synaptic activities by releasing ATP following spontaneous Ca^{2+} elevations (Halassa et al., 2007; Semyanov, 2019).

However, even the basic properties of ATP release, such as its spatial and temporal dynamics, remain unknown in physiological conditions due to limitations of detection methods. Non-optical approaches using the "sniffer cell" method, which sense extracellular ligands with artificially expressed receptors specific for target molecules combined with the patch-clamp technique or Ca^{2+} imaging, and microelectrode biosensors lack spatial information to reveal the dynamics of extracellular ATP at sub-cellular resolution (Wu & Li, 2020). Since they cannot identify individual release events, the temporal kinetics of ATP release also remains elusive. To overcome these technical difficulties, optical sensors have been developed. However, they were not adequate to detect endogenous ATP release in the brain tissue until recently (Conley et al., 2017; Lobas et al., 2019; Wu & Li, 2020). These limitations hampered clarification of the spatiotemporal properties of ATP release and their relationships with spontaneous Ca^{2+} activities.

We previously developed a highly sensitive genetically encoded extracellular ATP fluorescent sensor, $GRAB_{ATP1.0}$, and successfully detected individual spontaneous ATP release events in neuron–glia culture and inflammation-induced ATP release in vivo (Li et al., 2022; Wu et al., 2022). In this study, we monitored extracellular ATP under physiological conditions in vitro, in acute brain slices, and in the mouse brain using $GRAB_{ATP1.0}$. Furthermore, we investigated the spatiotemporal dynamics of spontaneous ATP release and its relationship with intracellular Ca^{2+} events in cortical astrocytes. Our results strongly suggest that astrocytes spontaneously and locally release ATP through multiple mechanisms, mainly in non-vesicular and Ca^{2+}-independent manners.

2 | MATERIALS AND METHODS

2.1 | Experimental design

All procedures were approved by the Committee on the Ethics of Animal Experiments of Waseda University and the Animal Care and Use Committees at Peking University. Wild-type ICR mice were maintained in Waseda University in accordance with the guidelines outlined by the Institutional Animal Care and Use Committee of Waseda University, and both male and female mice were used for experiments.

2.2 | DNA plasmid construction

Plasmid vectors based on the integration-coupled on (iOn) gene expression switch system conditioning transgene expression to piggyBac-mediated transposition (Kumamoto et al., 2020) were employed for stable expression of fluorescent sensors in astrocytes. To construct the *^{iOn}CAG∞GRAB$_{ATP1.0}$* plasmid, the $GRAB_{ATP1.0}$ coding sequence was amplified by PCR (primers: 5′; GTGGCCACTCGAGGATCCACCATGG AGAGAGACAC, 3′; GCACTAAAGTCGGATCAGAGGGGCGCTAGCTT ACA) and cloned into *^{iOn}CAG∞MCS* at the XhoI site by SLiCE cloning (Motohashi, 2015). *^{iOn}CAG∞REX-GECO1* was constructed by replacing the sequence between the BamHI and NheI sites of *^{iOn}CAG∞GRAB$_{ATP1.0}$* with the BamHI-XbaI fragment of *pCMV-REX-GECO1*. For the construction of *^{iOn}CAG∞Lck-REX-GECO1*, the Lck domain digested from *pCMV-Lck-MaLionR* with NheI and BamHI was inserted into the AvrII and BamHI sites of *^{iOn}CAG∞REX-GECO1*.

2.3 | In utero electroporation

Pregnant ICR mice were purchased from Japan SLC Inc. (Hamamatsu, Japan), and in utero electroporation (IUE) was performed as previously described (Li et al., 2020) with the following modifications. Mice at gestation day 15 were deeply anesthetized with either a mixture of medetomidine (0.3 mg/kg body weight), midazolam (4 mg/kg) and butorphanol (5 mg/kg) or with sodium pentobarbital (50 mg/kg) by intraperitoneal administration. Approximately 1 μL of plasmid solution containing 2.0 μg/μL of the iOn-switch vectors, 0.5 μg/μL of *pCAG-hyPBase* and 0.01% Fast Green solution (Sigma-Aldrich, Tokyo, Japan) was injected into a lateral ventricle of each embryo.

2.4 | Immunohistochemistry

$GRAB_{ATP1.0}$-expressing mice (4–8 weeks old), which had undergone IUE, were anesthetized with isoflurane (DS Pharma Animal Health Co. Ltd., Osaka, Japan) and transcardially perfused with phosphate-buffered saline (PBS) followed by 4% paraformaldehyde (PFA) in PBS (Nacalai Tesque, Kyoto, Japan). Brain samples were post-fixed in 4%

PFA at 4°C overnight and coronally sectioned at 150 μm thickness using a vibratome-type tissue slicer (DTK-1000, Dosaka-EM, Kyoto, Japan). The brain slices were then immersed in 0.3% Triton X-100 in PBS for 5 min at room temperature. After three time rinses with PBS, the slices were blocked with TNB blocking buffer [0.1 M Tris–HCl, 0.15 M NaCl, 0.5% TSA blocking reagent (PerkinElmer, Boston, MA, USA)] and incubated with a primary antibody (1:500 in TNB, goat polyclonal anti-GFAP antibody, ab53554, abcam, Cambridge, United Kingdom) and a secondary antibody (1:200 in TNB, Alexa 647 donkey anti-goat IgG, 705-609-147, Jackson ImmunoResearch Laboratories, Inc., West Grove, PA, U.S.A.). The cortical regions were observed using confocal microscopy (FV1000, Olympus, Tokyo, Japan). The mean fluorescence intensity was calculated using Image J (Schneider et al., 2012), and transfected and non-transfected hemispheres were compared.

2.5 | Cell culture

Rat primary neuron–glia co-cultures were prepared and cultured as described previously (Wu et al., 2022). In brief, co-cultures were prepared from 0-day-old (P0) wild-type Sprague-Dawley rat pups (male and female, randomly selected) purchased from Charles River Laboratories (Beijing, China). Hippocampal cells were dissociated from the dissected brains in 0.25% Trypsin-EDTA (Gibco, Waltham, MA, U.S.A.) and plated on 12-mm glass coverslips coated with poly-D-lysine (Sigma-Aldrich) in neurobasal medium (Gibco) containing 2% B-27 supplement (Gibco), 1% GlutaMAX (Gibco), and 1% penicillin-streptomycin (Gibco). Based on glial cell density, after approximately 4 days in culture (DIV 4) cytosine β-D-arabinofuranoside (Sigma-Aldrich) was added to the hippocampal cultures in a 50% growth media exchange, at a final concentration of 2 μM. Primary neuron–glia co-cultures were cultured at 37°C in 5% CO_2. To express $GRAB_{ATP1.0}$ in neurons, adeno-associated viruses (AAV2/9-hSyn-$GRAB_{ATP1.0}$) were added to neuron–glia co-cultures at DIV 5–9, and DIV ≥13 cells were used for imaging. Before imaging, the culture medium was replaced with Tyrode's solution containing: 150 mM NaCl, 4 mM KCl, 2 mM $MgCl_2$, 2 mM $CaCl_2$, 10 mM HEPES, and 10 mM glucose (pH 7.3–7.4). Cells grown on 12-mm coverslips were imaged using a Ti-E A1 confocal microscope (Nikon, Tokyo, Japan) equipped with a 10x/0.45 NA objective, a 20x/0.75 NA objective, a 40x/1.35 NA oil-immersion objective, a 488-nm laser, and a 561-nm laser; green fluorescence ($GRAB_{ATP1.0}$ sensors) and red fluorescence (Calbryte 590, AAT Bioquest) were recorded using a 525/50-nm, and 595/50-nm emission filter, respectively.

2.6 | Cranial window surgery

To minimize inflammatory responses, a thin skull surgery with optical clearing methods was employed to prepare a cranial window for in vivo imaging (Zhao et al., 2018). Mice were anesthetized with the anesthetic agents indicated above, and a metallic head plate (19 mm long, 12 mm wide, and 1 mm thick) with a hole (5 mm in diameter) was attached to the skull with dental cement (GC Corporation, Tokyo, Japan). The skull was thinned with a dental drill and then treated with 10% (W/V) Na_2EDTA (pH 7.0) for 30–40 min to decalcify the skull. The dip in the skull was filled with 80% glycerol, covered with a circular cover glass (4 mm in diameter, 0.12 mm in thickness, Matsunami, Osaka, Japan), and sealed with cyanoacrylate glue (Aron Alpha, Toagosei Co., Ltd, Tokyo, Japan).

2.7 | Acute slice preparation

Acute cortical slices were prepared from 4 to 8 weeks old mice which had undergone IUE. The brain was removed quickly and placed in an ice-cold cutting solution containing: 120 mM Choline-Cl, 3 mM KCl, 1.25 mM NaH_2PO_4, 26 mM $NaHCO_3$, 8 mM $MgCl_2$ and 20 mM D-glucose. Then, the brain was coronally sectioned at 350 μm thickness with a vibratome-type tissue slicer (Pro7, Dosaka-EM) and incubated for 1 h at 28°C for recovery in artificial cerebrospinal fluid (ACSF) containing: 124 mM NaCl, 2.5 mM KCl, 1.25 mM NaH_2PO_4, 26 mM $NaHCO_3$, 2 mM $MgCl_2$, 2 mM $CaCl_2$, 20 mM D-glucose, and continuously bobbled with 95% O_2/5% CO_2. All acute slice experiments were performed within 6 h after slice recovery to avoid the effects of inflammatory responses (Chai et al., 2017).

2.8 | Pharmacological treatments in acute slice experiments

Tetrodotoxin (TTX; 1 μM; 1 mM stock in 12.5 mM citrate; Latoxan Laboratory, Portes lès Valence, France), DL-Ba Fluorocitrate (FC; 100 μM; 5 mM stock in distilled water with $NaSO_4$ precipitation of barium as described in Paulsen et al., 1987; Sigma-Aldrich, St. Louis, MO, USA), bafilomycin A1 [2 μM; 10 mM stock in Dimethyl sulfoxide (DMSO); L C Laboratories, Woburn, MA, USA], Carbenoxolone (CBX; 100 μM; 100 mM stock in distilled water; Sigma-Aldrich), and 4-[(2-butyl-6,7-dichloro-2-cyclopentyl-2,3-dihydro-1-oxo-1H-inden-5-yl)oxy]-butanoic acid (DCPIB; 10 μM; 10 mM stock in DMSO; Cayman Chemical, Ann Arbor, MI, U.S.A) were each bath applied through superfusion of ACSF during recording sessions. FC and bafilomycin A1 were also pre-incubated for at least 2 h prior to recording. For intracellular Ca^{2+} buffering, slices were pre-incubated in ACSF containing BAPTA-AM (100 μM; 100 mM stock in DMSO; Nacalai Tesque) or its solvent, 0.1% DMSO (Sigma-Aldrich) and 0.02% Pluronic F-127 (Affymetrix, Maumee, OH, USA), as a control for 1 hour at 33–34°C prior to recording. For calibration of $GRAB_{ATP1.0}$ response in acute slice, ATP was bath-applied at 0.2, 0.5, 1, 5, 10, and 100 μM (Sigma-Aldrich), and astrocytes located at the surface of slices were monitored to avoid the rapid degradation of extracellular ATP by ectonucleotidases deep in the slice.

2.9 | Two-photon imaging

Imaging was performed with an in-house two-photon laser scanning microscope controlled by TI Workbench software (Inoue, 2018). $GRAB_{ATP1.0}$ and Lck-REX-GECO1 (Wu et al., 2014) were excited at 920 nm in acute slice experiments and at 860 nm in in vivo imaging using a titanium-sapphire pulse laser (Mai Tai DeepSee, Spectra-Physics, Tokyo, Japan) through a 20× objective (XLUMPLFLN20xW, Olympus) in acute slice experiments and through a 25× objective lens (XLPLN25xWMP2, Olympus) in in vivo imaging. The emissions were separated by a 580-nm beam splitter, passed through a 495–540 or 573–648-nm band pass filter, and detected with GaAsP-type photomultiplier tubes (H7422PA-40, Hamamatsu Photonics, Hamamatsu, Japan). The boundary of each fluorescent indicator-expressing astrocyte was easily identified when no adjacent cells expressed fluorescent probes. When two adjoining astrocytes were fluorescent, boundary of the two cells was discernible in many cases by taking image stacks from different focal depths, where expression levels of fluorescent probes apparently differed each other or the boundary was obvious by tracing the round edges of the two astrocytic territories. When the boundary of adjoining fluorescent astrocytes was not clear, further time-lapse imaging was not performed. Time-lapse image sequences in subregions adjusted for single astrocytes were acquired at 1 Hz with a 0.8 × 0.8 μm per pixel resolution, and line-scan images were acquired at 100 Hz. Astrocytes located 30–100 μm below the slice surface were monitored in acute slice experiments; in vivo, we imaged astrocytes located less than 140 μm from the brain surface. Each time-lapse recording session was taken for 30 min in each cell, except for the calibration of $GRAB_{ATP1.0}$ response and for the experiment with altered extracellular K^+ concentrations (20 min each for the three K^+ concentrations). In some cells in experiments where superfusate was not changed during the time course, recording sessions were repeated once.

2.10 | Event detection and overlap analysis in ATP and Ca^{2+} imaging

Background of time-lapse images was determined and subtracted in each image frame by taking the average of >200 pixels of no fluorescence of expressed sensors. Background-subtracted images were temporally smoothed with a three-frame-width moving average filter to reduce noise before event detection analysis in TI Workbench. Additionally, motion artifacts in some data were corrected by ImageJ plug-in StackReg (Thévenaz et al., 1998) implemented in TI Workbench. Processed image data were further analyzed with the Astrocyte Quantitative Analysis (AQuA) software (Wang et al., 2019) running in the MATLAB environment for event detection and event feature extraction of ATP and Ca^{2+} events with its masking and segmentation functions. Events of temporally less than three frames exceeding half peak height or spatially narrower than 32 pixels area for ATP events and 25 pixels area for Ca^{2+} events were ignored in event detection. The overlap between the ATP and Ca^{2+} events was determined by the following criteria (see also Figure S3): detected areas for ATP and Ca^{2+} events shared pixels; and event durations, defined as full width at 30% maximum, of both ATP and Ca^{2+} events overlapped with each other. The sequence of the ATP and Ca^{2+} events was then evaluated by the time point at 50% rise, and event pairs that showed a lag of one frame or less were defined as simultaneous events.

2.11 | Classification of ATP release events

To classify ATP release events according to the waveform of fluorescence trace, hierarchical clustering was conducted (see also Figure S5) in Python using NumPy, SciPy, and pandas libraries (Harris et al., 2020; McKinney, 2010; Virtanen et al., 2020). First, ATP events observed in acute slices, which were not treated with drugs, were collected. Each trace within time points from −40 to 120 frames relative to the 30% rise frame was extracted and scaled with z-score normalization to calculate the shape-based distance. Then, hierarchical clustering was performed based on the shape-based distance using the Ward's linkage method (Ward, 1963). The obtained clusters were used as training samples, and ATP release events observed in pharmacological experiments were classified using the nearest neighbor classification algorithm (Fixt & Hodges, 1951). To display the distribution of ATP event waveforms in 2D (Figure 5g, j), the principal component analysis (PCA) from scikit-learn library (Pedregosa et al., 2011) or the uniform manifold approximation and projection (UMAP) method (McInnes et al., 2018) was applied.

2.12 | Statistical analysis

Statistics were performed using Python 3.7 and R (RStudio 1.2.5042) and are described in the corresponding figure legends. All tests were two-tailed, and a *p*-value lower than .05 was considered significant. Data following normal distribution were represented as means ± SD with bar plots, and paired t-tests were applied. When normal distribution cannot be assumed, results were represented as the median and interquartile range (IQR) [25th and 75th percentile] with box plots. Mann–Whitney *U* test and the Wilcoxon signed-rank test were used for a two-group comparison of unpaired and paired data, respectively. In more than three-group comparisons, Steel-Dwass test and Friedman test were used for unpaired and paired data, respectively. The correlation coefficients were calculated using Kendall's correlation test, a nonparametric method resistant to equal ranking. For evaluating the effect of inhibitors on the frequency of ATP release events assigned to each cluster, *p*-values were calculated from the Poisson distribution, and Bonferroni correction was used for the drug-free versus DMSO vs BafA1 comparison. For assessing the significance of overlapping pattern incidence and Ca^{2+} activity before and after

ATP release events, the chance level was calculated by randomly shuffling the event onsets.

3 | RESULTS

3.1 | Spontaneous ATP release in neuron-glia co-culture is independent of neuron activity

We have previously reported that ATP release is detected without external stimulations in rat primary neuron–glia co-culture expressing $GRAB_{ATP1.0}$ (Wu et al., 2022). To test whether neuronal activity participates in this spontaneous ATP signaling, we first blocked neuron firing with tetrodotoxin (TTX). The frequency and amplitude of spontaneous ATP release events were not significantly altered by the TTX treatment, while the responses were abolished by application of the P2Y1 receptor antagonist MRS-2500, as expected from the fact that the sensor originated from the human P2Y1 receptor (Figure 1a–d). When the neuronal activity was enhanced by electrical stimulation and high K^+ treatment, robust Ca^{2+} elevation in neurons was induced, while no increased $GRAB_{ATP1.0}$ response was detected. The application of 100 nM ATP was sufficient to evoke a robust $GRAB_{ATP1.0}$ response (Figure 1e–g). Altogether, these results demonstrated that neuronal activity was not responsible for the spontaneous ATP release observed in rat primary neuron–glia co-culture.

3.2 | Cortical astrocytes spontaneously and locally release ATP

To monitor extracellular ATP dynamics in murine brain tissue, astrocytes expressing $GRAB_{ATP1.0}$ were prepared by means of in utero electroporation with an improved transposon vector based on the iOn-switch (Kumamoto et al., 2020) (Figure 2a). This approach achieved sparse expression of the ATP sensor in cerebral cortex and enabled us to distinguish individual astrocytes by morphology (Figure 2b). Neither glial scar formation nor upregulation of glial fibrillary acidic protein (GFAP) expression was observed (Figure S1), suggesting no detectable inflammatory activation of astrocytes.

We then monitored $GRAB_{ATP1.0}$ fluorescence in single astrocytes in anesthetized mice using two-photon microscopy. During the 30-min recording sessions, overall 12 transient increases in extracellular ATP were observed in 8 out of 30 cells from 6 mice within restricted subcellular regions (Figure 2c–e; frequency: 2.2×10^{-4} Hz/cell; area: 124.16 [37.28, 381.6] μm^2; full width at half maximum (FWHM): 6 [5, 14] s; peak $\Delta F/F_0$: 51.4% [41.7%, 65.8%]; median [interquartile

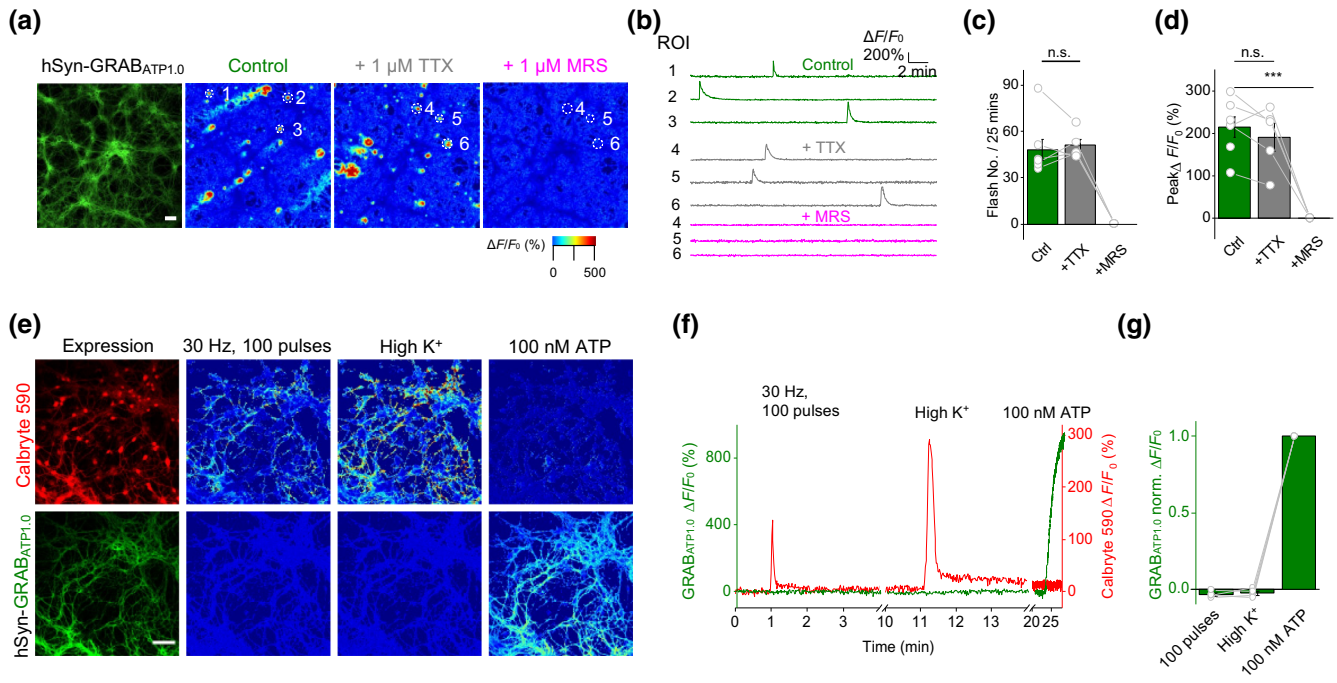

FIGURE 1 TTX-insensitive spontaneous ATP release in rat hippocampal neuron–glia co-culture. (a) Raw fluorescence image and pseudocolor images of the fluorescence response ($\Delta F/F_0$) of $GRAB_{ATP1.0}$ in Tyrode's solution (control), tetrodotoxin (TTX, 1 μM), and MRS-2500 (a P2Y1R antagonist, MRS, 1 μM). (b) Time course traces of the fluorescence response ($\Delta F/F_0$) of $GRAB_{ATP1.0}$ in the regions of interest (ROI) circled in (a). (c, d) Frequency (number of events per 25 min (c) and peak amplitude (d) of fluorescence transients recorded from 4 to 6 coverslips. (e) Images of Calbryte 590 (top) and $GRAB_{ATP1.0}$ (bottom) showing raw fluorescence, $\Delta F/F_0$ on field electrical stimulation (100 pulses at 30 Hz), high K^+ stimulation and 100 nM ATP application, from left to right. (f) Time course traces showing the mean fluorescence response ($\Delta F/F_0$) in the field of view of Calbryte 590 (red) and $GRAB_{ATP1.0}$ (green) to the stimulations. (g) Peak amplitudes of $GRAB_{ATP1.0}$ fluorescence responses recorded from 3 coverslips. Scale bars: 100 μm (a) and 30 μm (e). Student's *t*-test, ***$p < .001$; n.s., not significant.

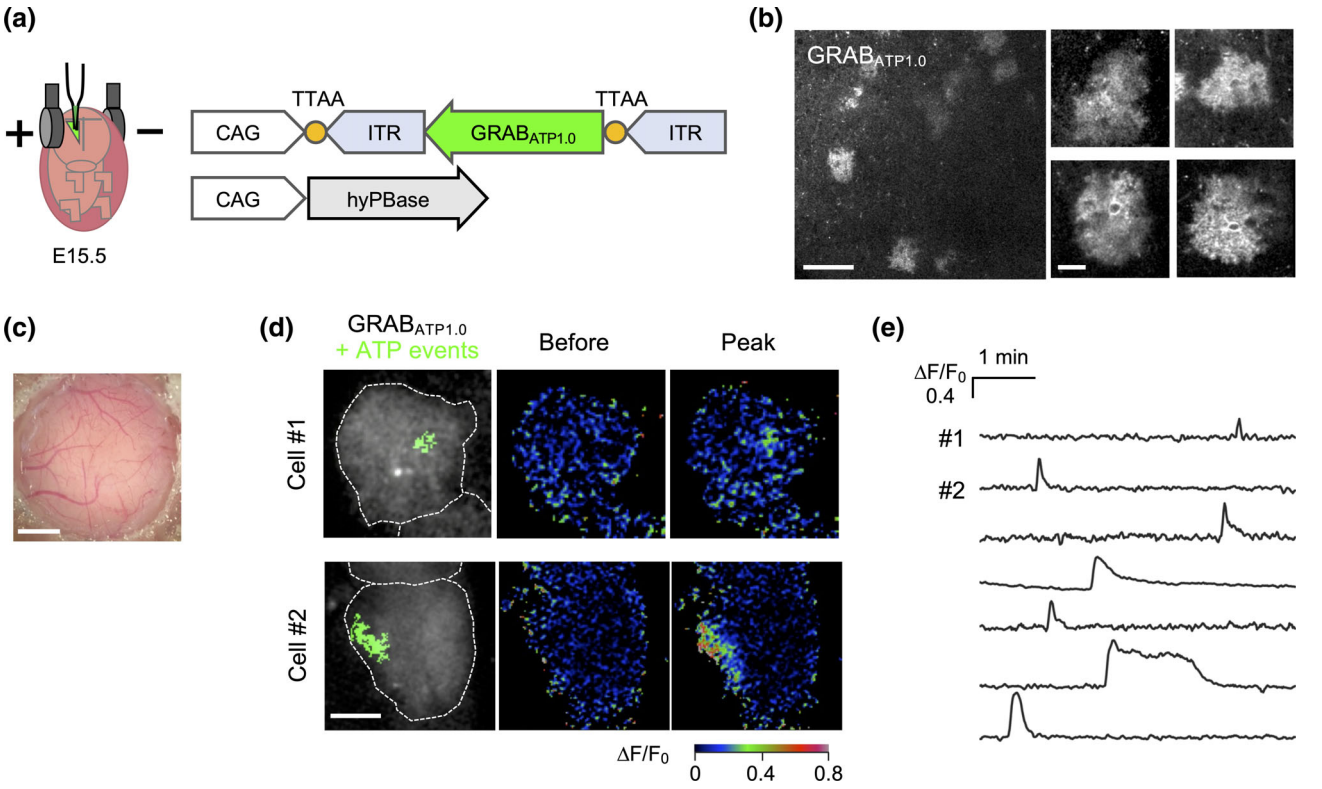

FIGURE 2 Local and transient ATP release in vivo. (a) Schematic drawing of in utero electroporation and plasmids for expressing $GRAB_{ATP1.0}$ with the iOn-switch PiggyBac transposon system. (b) Images of cortical slices prepared from P40 mice electroporated at E15.5 showing $GRAB_{ATP1.0}$ fluorescence expressed in a small number of astrocytes. High-magnification images (right) were taken from the same slice with different focal planes. (c) A thinned-skull cranial window. (d) Focal spontaneous ATP release events in astrocyte arbors in vivo. $GRAB_{ATP1.0}$ fluorescence images of two astrocytes (left). ATP increase areas detected by AQuA software (Wang et al., 2019) are shown in green, and astrocyte borders are indicated by dashed lines. $\Delta F/F_0$ images of $GRAB_{ATP1.0}$ before (middle) and during (right) the spontaneous ATP events. (e) Time course traces of $GRAB_{ATP1.0}$ signals ($\Delta F/F_0$) showing ATP release events. Traces marked as #1 and #2 correspond to the events shown in (d), and the others were obtained in different cells. Scale bars: 100 μm (b, left), 20 μm (b, right, and d), and 1 mm (c).

ranges (IQRs)]). Such transient and localized ATP events were also found in acute brain slices without stimulation (28 events in 14 cells in 14 slices from 4 mice; frequency: 1.1×10^{-3} Hz/cell; area: 111.68 [49.92, 263.68] μm^2; FWHM: 23 [11, 62.5] s; peak $\Delta F/F_0$: 160.5% [116.6%, 227.2%], see the control group in Figure 3a–c, f–h). To identify the source of spontaneous ATP release in slices, the activities of neurons and of astrocytes were suppressed by TTX and an astrocyte-specific gliotoxin, FC, respectively. ATP release events were insensitive to TTX concerning their frequency, area, duration, and peak amplitude (Figure 3c–h), consistent with the results in neuron–glia co-cultures. By contrast, the frequency of ATP release was suppressed by FC (Figure 3i, j), indicating that the spontaneous ATP release in the brain slice was dependent upon the astrocyte activity. These results indicate that cortical astrocytes release ATP independently of neuronal activity.

To estimate the concentration of locally released ATP, the $GRAB_{ATP1.0}$ response in slice was calibrated by bath-application of ATP (Figure 3k, l). With this calibration result and the peak amplitudes of ATP release events (Figure 3g), the peak concentration of typical ATP release appeared to range between 0.5 and 5 μM, which meets the concentration range for activation of purinergic receptors (Khakh & North, 2012; Vitiello et al., 2012), indicating that spontaneous ATP release may affect multiple synapses within the local areas all at once.

3.3 | The majority of spontaneous ATP release do not coincide with Ca^{2+} elevation in astrocytes

To examine the relationship between spontaneous ATP release and Ca^{2+} activity in astrocytes, we monitored extracellular ATP and intracellular Ca^{2+} dynamics simultaneously by expressing $GRAB_{ATP1.0}$ and a membrane-anchored red Ca^{2+} sensor, Lck-REX-GECO1 (Wu et al., 2014), in astrocytes in acute brain slices (Figure 4a). We detected 165 ATP- and 4,760 Ca^{2+}- events from 56 cells in 53 slices from 18 mice (1.3×10^{-3} and 39×10^{-3} Hz/cell, respectively; 12 of the 56 cells were recorded twice). Of note, the frequency of Ca^{2+} transients did not increase over time during the 30-min recording session (Figure S2), ruling out the possibility of photo-damage caused by two-photon excitation (Schmidt & Oheim, 2020). The rise time, fall time, FWHM of duration, and area of ATP events were relatively more broadly distributed than those of Ca^{2+} events (Figure 4b–e). In

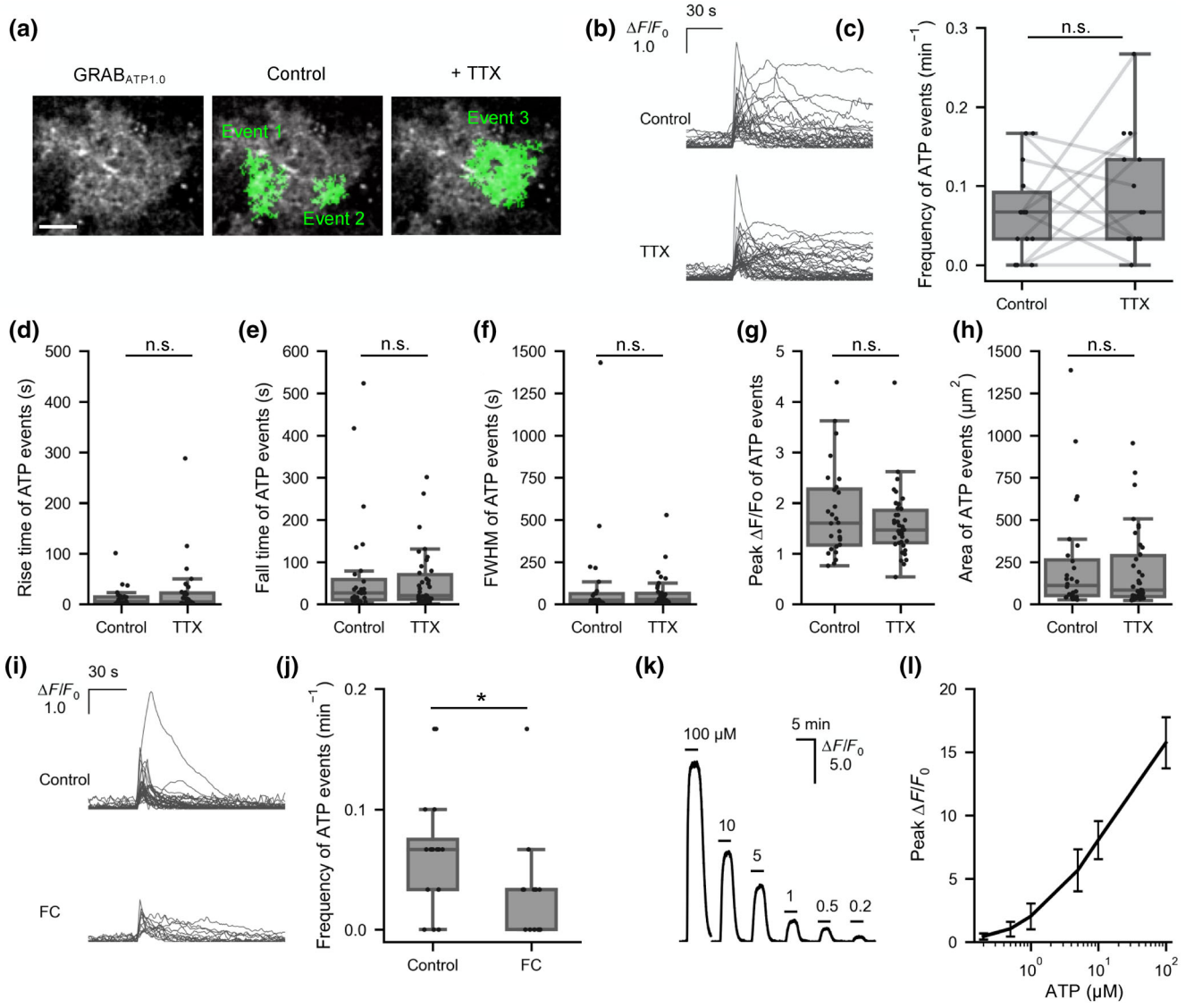

FIGURE 3 Astrocytes spontaneously release ATP in acute slices. (a) A cortical astrocyte in an acute slice expressing GRAB$_{ATP1.0}$ (left) overlayed with focal spontaneous ATP release events (green) observed in control (middle) and in 1 μM TTX (right) conditions. Scale bar: 20 μm. (b) Time course changes in GRAB$_{ATP1.0}$ signal ($\Delta F/F_0$) of spontaneous ATP release events detected in control (top, $n = 28$ events in 14 slices from 4 mice) and in TTX (bottom, $n = 38$ events in 14 slices from 4 mice) conditions. Events are aligned by the initial rise timing (30% of the peak amplitude). (c) Frequency of spontaneous ATP release events ($n = 14$ cells each). (d–h) Rise time (d), fall time (e), full width at half maximum (FWHM) of duration (f), peak amplitude of $\Delta F/F_0$ (g), and area (h) of spontaneous ATP release events in control and TTX groups. (i) Time course changes in GRAB$_{ATP1.0}$ signal ($\Delta F/F_0$) of spontaneous ATP release events detected in control ($n = 32$ events in 16 cells from 4 mice) and fluorocitrate (FC, 100 μM; $n = 13$ events in 15 cells from 4 mice) conditions. (j) Frequency of spontaneous ATP release events in the control and FC groups. (k) $\Delta F/F_0$ changes of GRAB$_{ATP1.0}$ expressed in an astrocyte in acute slice responding to bath-application of 100, 10, 5, 1, 0.5, and 0.2 μM ATP. (l) Calibration of the response of GRAB$_{ATP1.0}$ expressed in astrocytes in acute slice (mean ± S.D, $n = 5$ cells). Wilcoxon signed-rank test (c) and Mann–Whitney *U* test (d–h and j) were used. Box plots show the median, 25th, and 75th percentile.

contrast, the peak amplitude and subcellular location of ATP and Ca^{2+} events were distributed similarly (Figure 4f, g). Unexpectedly, more than half of the spontaneous ATP release events did not coincide with Ca^{2+} elevation (Figure 4k). ATP release events devoid of Ca^{2+} events were also detected through line-scanning at a 100 Hz sampling rate (Figure S4). Among the spatially overlapping patterns, ATP events followed by Ca^{2+} elevation (Figure 4h) were most frequently observed, and the incidences of ATP events following or coinciding with Ca^{2+} elevation were low (Figure 4i, j). The occurrence of ATP events preceding or following Ca^{2+} events was not statistically significant, although that of the coinciding events was above chance-level ($p < .001$; Figure 4k). Besides, Ca^{2+} events occurred with significantly higher frequency only during the 30-s period just after the ATP release events (Figure 4l). The frequency of Ca^{2+} events per cell did not correlate with that of spontaneous ATP events (Figure 4m). These results suggest that most of the spontaneous ATP release occurred in

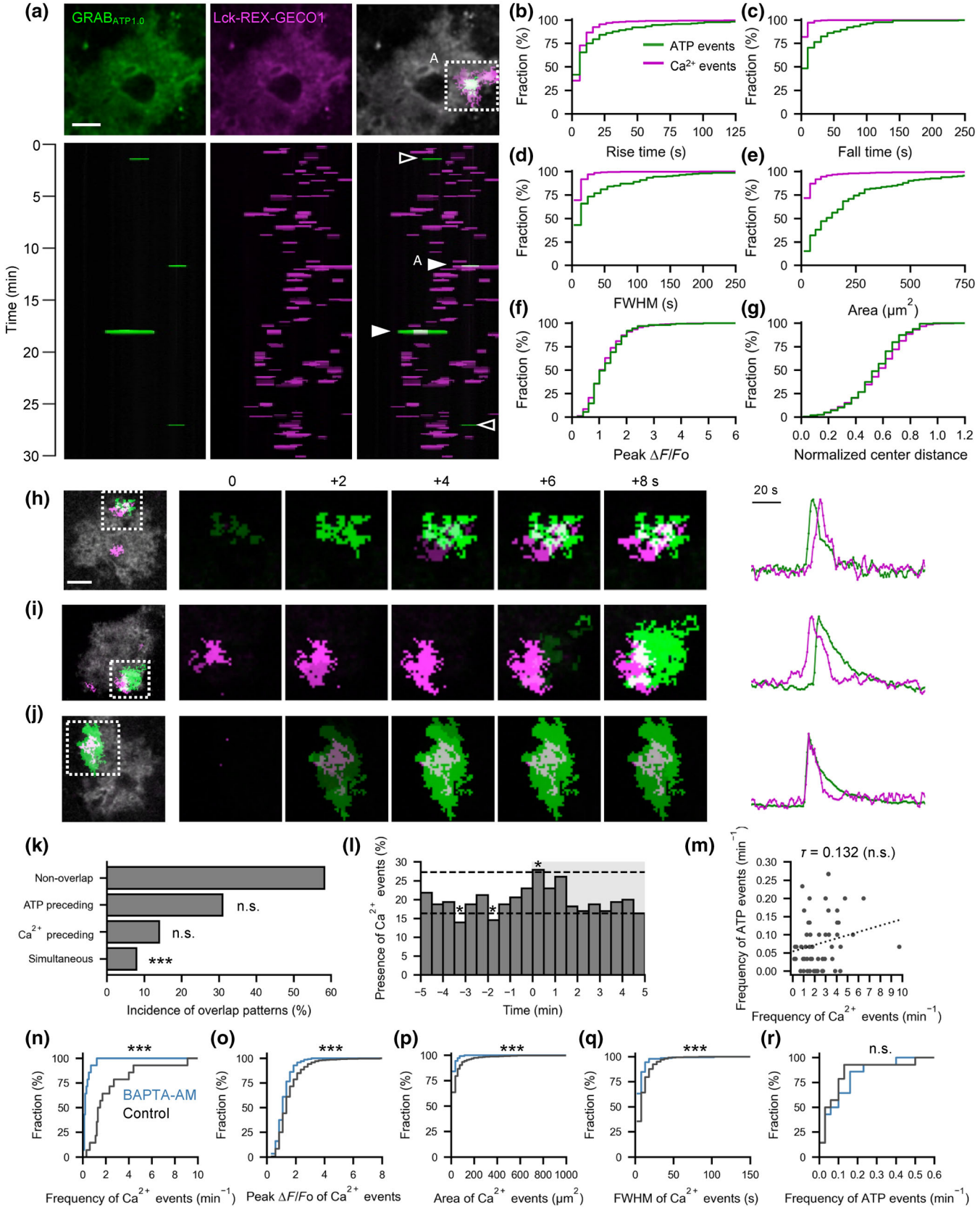

FIGURE 4 Legend on next page.

a Ca^{2+}-independent manner. To further test this notion, acute slices were incubated in 100 μM BAPTA-AM, a cell membrane-permeable intracellular Ca^{2+} chelator, for 1 h just before recording. While the frequency, peak $\Delta F/F_0$, area, and duration of Ca^{2+} events were drastically reduced by the BAPTA-AM treatment ($n = 144$ Ca^{2+} events in 14 cells from 3 mice) compared to those in the control condition ($n = 1{,}001$ Ca^{2+} events in 14 cells from 3 mice; Figure 4n–q), no significant difference was observed in the frequency of ATP events (Figure 4r). Altogether, these results demonstrate that astrocytes spontaneously release ATP in a Ca^{2+}-independent manner.

3.4 | ATP release events can be classified into five clusters based on the waveform

Vesicular release and release through several channels have been proposed as candidate mechanisms for ATP release from astrocytes (Illes et al., 2019). Because spontaneous ATP release events appeared to vary kinetically (Figures 3b and 4b–d), we presumed that their waveforms might reflect distinct ATP release mechanisms. To classify ATP events according to their waveforms, hierarchical clustering was conducted using a shape-based distance (SBD) algorithm based on normalized cross-correlation (Paparrizos & Gravano, 2015) (Figure S5). Two classes and five subdivided clusters were determined, and ATP events in the primary class (class 2) had sharper waveforms than the other class (Figure 5a, b). Additionally, non-linear dimensionality reduction by the uniform manifold approximation and projection (UMAP) algorithm (McInnes et al., 2018) clearly showed gaps among the clusters determined by hierarchical clustering, except for clusters iii (brown) and v (purple; Figure 5j). Altogether, these analyses revealed that the spontaneous ATP release from astrocytes comprises multiple groups presenting distinct kinetics.

We then examined the relationship between ATP and Ca^{2+} events in each cluster. We found that only the ATP events in cluster ii tended to accompany Ca^{2+} events before and just after the ATP events (Figure 5c), which was buried in the overall analysis (Figure 4l). This implies that ATP event types classified by the waveform reflect different mechanisms that lead to different ATP kinetics. No apparent difference was found in peak amplitude and area of ATP events among the clusters (Figure 5d, e), suggesting that the amount of released ATP may be irrelevant to the distinct effects of ATP clusters on the Ca^{2+} events. Also, preference for the subcellular location of ATP release was not observed among the clusters (Figure 5f).

3.5 | A minority of ATP events characterized by slow kinetics correspond to vesicle release

To verify the possibility that the difference in the waveform of ATP events reflects distinct release mechanisms, ATP events observed in the presence of inhibitors against vesicular release (2 μM bafilomycin A1, BafA1, >2 h pre-incubation and bath-application, $n = 46$ events from 22 cells) and its control (0.1% DMSO, $n = 49$ events from 23 cells), hemichannels (100 μM carbenoxolone, CBX, $n = 48$ events from 22 cells), and volume-regulated anion channels (10 μM DCPIB, $n = 52$ events from 22 cells) were similarly classified using the nearest neighbor classification algorithms with the SBD measure. Hemichannels were reported to participate in ATP release in the resting state of hippocampal slices (Chever et al., 2014). Notably, the frequency of ATP events belonging to class 1 decreased under BafA1 treatment, but not in the DMSO-treated control groups (Figure 5g, h). Also, the BafA1 treatment abolished ATP events assigned to cluster i (Figure S6). These results suggest that the class 1 ATP release events characterized by a slow time course are driven by vesicular release. In contrast, treatment with CBX showed no apparent changes in any of the classes or clusters, suggesting that the contribution of connexin and pannexin hemichannels is minimal in cortical slices (Figures 5g, h, and S6). In the DCPIB group, shifts in the frequency of ATP events assigned to class 1 and 2 were insignificant, however, the frequency of cluster v events decreased and that of cluster iii events

FIGURE 4 Simultaneous imaging of spontaneous ATP release and Ca^{2+} activity in astrocytes in acute slices. (a) X–T binary maps showing overlays (maximal values on the *y*-axis) of spontaneous ATP release events (bottom left), spontaneous Ca^{2+} events (bottom middle), and the both (bottom right) detected from an astrocyte expressing $GRAB_{ATP1.0}$ (top left) and Lck-REX-GECO1 (top middle). ATP events occurred with (close arrowhead; X–Y images of the both events (A) are overlaid in the top right image) or without (open arrowhead) accompanying Ca^{2+} events at the same time. (b–g) Cumulative frequency curves showing the distribution of rise time (b), fall time (c), FWHM of duration (d), area (e), peak amplitude in $\Delta F/F_0$ (f), and distance between the gravity center of event area and the gravity center of astrocyte area normalized by the cell radius (g) of spontaneous Ca^{2+} transients (magenta, $n = 4{,}760$ events) and ATP release events (green, $n = 165$ events). The numbers of events out of the abscissa range are 2, 2, 2, 8, 0, and 0 in the ATP events and 24, 1, 1, 19, 2, and 3 in the Ca^{2+} events in (b–g), respectively. (h–j) Three representative data showing overlapping ATP release and Ca^{2+} events (top, an ATP event preceding a Ca^{2+} event; middle, an ATP event following a Ca^{2+} event; bottom, simultaneous events) in sequential images (left) and time course traces of $\Delta F/F_0$ (right). (k) Incidences of spontaneous ATP release events classified by temporal overlapping patterns with Ca^{2+} events. Chance levels (***$p < .001$; n.s., not significant) were estimated by shuffling the onset time of Ca^{2+} events (10,000 iterations). (l) The proportion of ATP release events in which Ca^{2+} events were observed in 30-s time windows. The onset of ATP release events corresponds to time 0. Chance levels (dashed lines, 95%) were estimated by shuffling the onset time of Ca^{2+} events (10,000 iterations). (m) Correlation between the frequency of spontaneous ATP release events and that of Ca^{2+} transients (Kendall's rank correlation, $n = 55$ cells). (n–r) Cumulative frequency curves showing frequency (n), peak amplitude of $\Delta F/F_0$ (o), area (p), and FWHM of duration (q) of Ca^{2+} events and frequency of ATP events (r) after treatment with BAPTA-AM (100 μM; $n = 46$ events in 14 cells from 3 mice) or control (0.1% DMSO and 0.02% Pluronic F-127; $n = 39$ events in 14 cells from 3 mice). Mann–Whitney *U* test. Scale bars: 20 μm.

increased (Figures 5g, h, and S6), implying that class 2 may include DCPIB-sensitive mechanisms. Note that the ATP release events that simultaneously occurred with Ca^{2+} events mostly belonged to class 2 (Figure 5i; 12 out of 13 simultaneous events), implying that they correspond to channels permeable to both ATP and Ca^{2+}, or rely on Ca^{2+}-dependent ATP channel opening, though their occurrence was low (12 out of 129 ATP events in class 2). Such simultaneous events were also detected under CBX (5 out of 48 total ATP events), all of

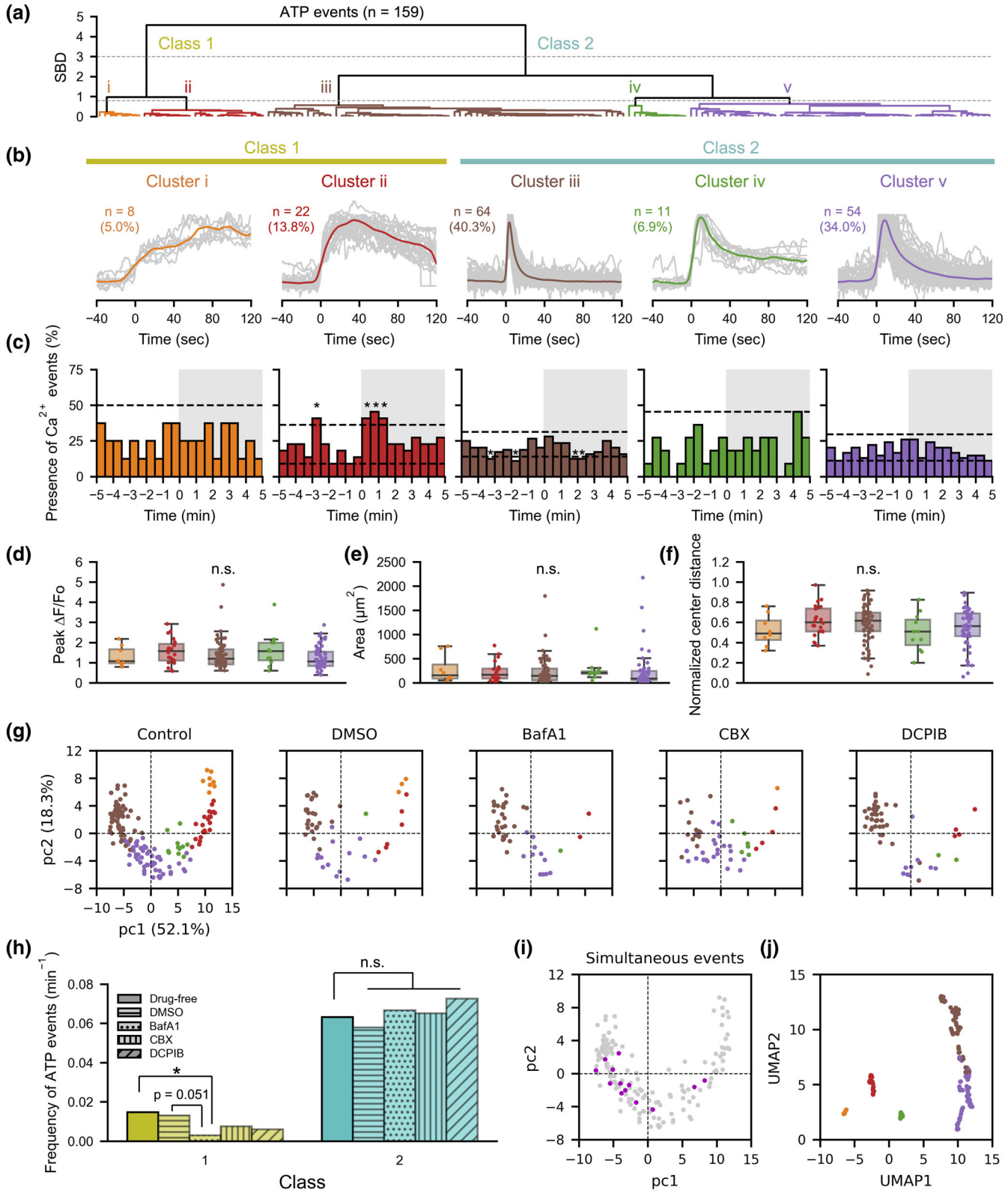

FIGURE 5 Legend on next page.

which were assigned to class 2, and the frequency among total ATP events (10.4%) was even larger than that in the normal condition without CBX (7.9%, Figure 4k).

Since cortical astrocytes exhibit heterogeneity in resting membrane potential (Morel et al., 2019) and some ATP release mechanisms are sensitive to membrane potential (Taruno, 2018), we investigated the effect of depolarization and hyperpolarization in astrocytes by switching the perfusate from regular K^+ (2.5 mM) ACSF to low K^+ (0.5 mM) then to high K^+ (10 mM) ACSF (Figure S7). Little changes were observed in the ATP event frequency among the K^+ conditions when each ATP event class or cluster was compared or overall ATP events were compared, indicating that shifts in extracellular K^+ concentration of the above range were less likely to determine the frequency of certain types of ATP release.

4 | DISCUSSION

In this study, we monitored spontaneous extracellular ATP dynamics using $GRAB_{ATP1.0}$ in neuron–glia co-culture, acute brain slices, and live brain. With the high sensitivity and spatiotemporal resolution of the sensor, ATP release events were spatiotemporally detected without stimuli in the three preparations. We then investigated the mechanisms of the spontaneous ATP release in acute slice and obtained three major findings: first, astrocytes release ATP independently of nearby neuronal activities; second, dual-color imaging revealed that ATP release events rarely coincide with a spontaneous Ca^{2+} transient and are resistant to Ca^{2+} buffering with BAPTA-AM; and finally, clustering analysis suggested that the spontaneous ATP release events involve multiple mechanisms with non-vesicular release being the major one, and that long-lasting ATP release is driven by exocytosis.

4.1 | Astrocyte actively drives purinergic signaling

Tonic extracellular purinergic signaling deriving from astrocytes in unstimulated brain slices has been reported (Chever et al., 2014; Kamatsuka et al., 2014), but whether astrocytes release ATP in a spontaneous fashion or as a consequence of basal neuronal activity has not been elucidated. To clarify this, we utilized FC, a metabolic inhibitor widely used as gliotoxin, which is selectively taken up by astrocytes. Though a study reports an acute reduction of excitatory synaptic transmissions in slice incubated with 200 μM FC for 30 min (Bonansco et al., 2011), others reported negligible effects on neuronal properties including membrane potential, input resistance, and amplitude of excitatory transmission with the same dose of FC incubation for several hours (Berg-Johnsen et al., 1993; Stone et al., 1990). In the present study, we showed that spontaneous ATP release in slice was TTX-insensitive but significantly suppressed by FC (100 μM, incubation for more than 2 h), demonstrating that astrocytes release ATP independently of neuron activity, and thus further prompting the notion that astrocytes can provoke active communications via gliotransmission spontaneously in addition to their classical role as passive elements of neuronal processing.

4.2 | Spatial properties of ATP release from astrocytes

Despite the morphological hallmarks where individual astrocytes interact with tens of thousands of synapses within their arbor territories, the spatiotemporal properties of gliotransmitter release have not been determined due to the limitations of detection methods. Our extracellular ATP imaging approach using $GRAB_{ATP1.0}$ revealed that spontaneous ATP release events typically spread over 50–250 μm^2 at a concentration of 0.5–5 μM in the slice. Considering the synapse density in the murine cortex (~0.7 synapses/μm^3; (Halassa et al., 2007; Kikuchi et al., 2020)) and EC_{50} of purinergic receptors (i.e., P2X1: 0.07; P2X2: 1.2; P2X3: 0.5; P2X4: 10; P2Y1: 8 μM; (Khakh & North, 2012; Vitiello et al., 2012)), our results indicate that individual ATP release events can potentially affect hundreds of nearby synapses all together even in a single focal plane. Halassa et al. speculated that gliotransmission groups adjacent synapses into functional ensembles because Ca^{2+} elevation that triggers gliotransmitter release is confined to subcellular regions in astrocytes (Halassa et al., 2007). The present results on ATP show that most of the

FIGURE 5 Clustering analysis of spontaneous ATP release events based on waveform. (a) Spontaneous ATP release events were classified into two classes and five sub-divided clusters by hierarchical clustering based on the waveform. (b) Gray lines indicate traces normalized by the peak amplitude of $\Delta F/F_0$, and colored lines represent the barycenter of traces belonging to the cluster. (c) The proportion of ATP release events in which Ca^{2+} events were observed in 30-s time windows. The onset of ATP release events corresponds to time 0. Chance levels (dashed lines, 95%) were estimated by shuffling the onset time of Ca^{2+} events (10,000 iterations). (d–f) The peak amplitude of $\Delta F/F_0$ (d), area (e), and distance between the gravity center of event area to the gravity center of cell area normalized by the cell radius of ATP release events in each cluster (median, and 25th and 75th percentile; Mann–Whitney *U* test). (g) Distribution of ATP release event waveforms in 2D by reducing the dimensions with the principal component analysis. The first and second principal components (pc1 and pc2) indicate 52.1% and 18.3% of explained variance, respectively. Colors correspond to those of the clusters in (a). (h) Effects of inhibitors on the ATP release event frequency in the two classes (control: $n = 55$ cells from 18 mice; DMSO: $n = 23$ cells from 6 mice; Bafilomycin A1 (BafA1, 2 μM): $n = 22$ cells from 7 mice; Carbenoxolone (CBX, 100 μM): $n = 22$ cells from 5 mice; DCPIB (10 μM): $n = 22$ cells from 3 mice; statistics: Poisson distribution). (i) ATP release events occurring simultaneously with Ca^{2+} transients (13 events) are colored magenta, and others gray in the same scatter plot shown in (g) (Control). (j) Distribution of the ATP release event waveforms displayed by reducing the dimensionality using the uniform manifold approximation and projection (UMAP) method. *$p < .05$; n.s., not significant.

release events of this particular gliotransmitter do not accompany Ca^{2+} events but that their spread is indeed localized. Thus, the conclusion by Halassa et al. that adjacent synapses form functional groups by local gliotransmission sounds valid. It should be noted, however, that $GRAB_{ATP1.0}$ captures both ATP and its degradation product, ADP (Wu et al., 2022). Therefore, the spatial and temporal spread of ATP, not ADP, could be smaller than that estimated in this study.

4.3 | ATP-induced Ca^{2+} response in astrocytes

It is reported that extracellularly released ATP induces astrocytic Ca^{2+} propagation in culture (Guthrie et al., 1999; Koizumi et al., 2003) and in pathological conditions in vivo (Delekate et al., 2014). It evokes an astrocytic Ca^{2+} response in an autocrine fashion in the brain slice (Shen et al., 2017). Our result showing that the frequency of Ca^{2+} activity slightly increased just after ATP release (Figure 4l) may reflect such ATP-induced Ca^{2+} response, though only in a quarter of the entire ATP release events observed, suggesting that spontaneously released ATP has little impact on astrocytic Ca^{2+} dynamics in the physiological slice condition. Our clustering analysis suggests that the spontaneous ATP gliotransmission involves multiple types of release machinery, and cluster ii only showed an enhancement of Ca^{2+} activity after ATP release (Figure 5c), which led us to presume that distinct ATP release mechanisms govern different downstream effects and also cooperatively engage in basal purinergic signaling.

4.4 | Mechanisms of spontaneous ATP release from astrocytes

Our pharmacological results suggest that ATP release events of relatively slow kinetics (class 1) are driven by vesicular ATP release. The slower decay phase of class 1 events could be explained by slower ATP diffusion, slower ATP degradation by ectonucleotidase, and long-lasting ATP release. Since it is hard to imagine that the conditions of ATP diffusion and degradation differ much in the extracellular space, long-lasting ATP release sounds reasonable. The asynchronous vesicle fusion mechanism, which does not accompany an active zone-like structure or a pool of vesicles (Aten et al., 2022), fits with such a release pattern. Studies directly monitoring vesicular ATP release in astrocyte culture reported several minutes lags between evoked Ca^{2+} elevation and resultant exocytosis. Of note, the occurrence of Ca^{2+} events in cluster ii of class 1 was high during the 30-s period 3 min before the ATP events (Figure 5b), which may indicate that cluster ii is driven by Ca^{2+}-triggered exocytosis. Then, given that most of the Ca^{2+} events were not accompanied by ATP release (Figure 4a), a yet-known triggering mechanism for such asynchronous vesicular ATP release other than the Ca^{2+} signal can be presumed. Alternatively, specific spatiotemporal patterns and/or strength of the Ca^{2+} signal could be effective. Besides, cluster i in class 1 is probably attributed to Ca^{2+}-independent exocytosis, which is also reported in the study of astrocyte culture (Li et al., 2015). Thus, the mechanisms evoking vesicular ATP release from astrocytes remain an open question.

On the assumption that the class 2 ATP release identified in this study represents channel-mediated ATP release, we can infer that this mechanism predominates over exocytosis (class 1; Figure 5a) in the basal purinergic signaling. It has been postulated that channel-mediated ATP release engages under pathological conditions (Giaume et al., 2013; Sahlender et al., 2014). However, accumulating evidence suggests that these mechanisms are also involved in basal ATP gliotransmission (Chever et al., 2014; Chi et al., 2022; Jun et al., 2018; Prochnow et al., 2012; Stehberg et al., 2012). While connexin hemichannels (Chever et al., 2014), pannexin 1 (Prochnow et al., 2012; Suadicani et al., 2012), calcium homeostasis modulator 2 (Jun et al., 2018), volume-regulated anion channels (Fujii et al., 2017), and maxi-anion channels (Liu et al., 2008) have been identified as ATP release channels in astrocytes, results in this study with CBX (Figure 5h) indicate that connexin hemichannels and pannexin 1 are less plausible candidates for the spontaneous ATP release events in the cortex. By contrast, DCPIB, a volume-regulated anion channel blocker, affected the appearance frequencies of the ATP event clusters iii and v (Figures 5g and S6), implying that class 2 may include DCPIB-sensitive mechanisms. We assume that the primary ATP release channel in the cortex is one of the anion-selective channels because of the very low incidence of synchronous Ca^{2+} and ATP events. To date, however, the molecular identity of these anion channels has not been fully elucidated, and there are no specific blockers validated in brain slice, especially for maxi-anion channels. Further studies on ATP release channels are needed to understand the molecular mechanisms underlying the spontaneous ATP release from astrocytes.

Our results showing that intracellular Ca^{2+} elevation is less likely responsible for the spontaneous ATP release events except for those in cluster ii, indicate that Ca^{2+}-independent processes may play crucial roles in the basal purinergic signaling. Various environmental changes such as decrease and increase in extracellular Ca^{2+} and K^+ concentrations, respectively, cell swelling, low oxygen, and mechanical transduction have been demonstrated to open ATP release channels (Taruno, 2018), while it is not clear whether actual changes in those parameters are sufficient to affect ATP release channels under physiological conditions. At least, concentrations of extracellular K^+ in the range of 0.5–10 mM, corresponding to membrane potential shifts ranging from −20 to +23 mV (Figure S7), did not appear to affect spontaneous ATP release from astrocytes. Besides, intracellular Ca^{2+} events could still be candidates for ATP release: faint nanoscale Ca^{2+} events in the astrocyte structure only detectable by STED microscopy (Arizono et al., 2020), fast Ca^{2+} events (FWHM <1.5 s, Bindocci et al., 2017), or out-of-focus Ca^{2+} events might have been missed in this study. Thus, future studies employing advanced optical techniques including super-resolution microscopy and volumetric multi-photon imaging might help uncover the mechanisms underlying the spontaneous ATP release from astrocytes in space and time.

4.5 | Physiological significance of spontaneous ATP release

To date, few reports have been published on the physiological significance of the spontaneous ATP release from astrocytes. Pioneering studies on spontaneous ATP release in neuron–glia co-culture reported that extracellular ATP suppresses the excitatory neuron activity through presynaptic P2Y receptors, and 0.3–3 μM of extracellularly applied ATP was sufficient to attenuate synaptic release (Koizumi et al., 2003; Zhang et al., 2003). As for evoked-ATP release, ATP upregulates the activity of CCK-positive interneuron via presynaptic P2Y1 receptor while downregulating pyramidal neuron activity mediated by its metabolite adenosine (Tan et al., 2017), and it attenuates inhibitory postsynaptic currents via postsynaptic P2X2 and P2X4 receptors (Lalo et al., 2014) in the slice. In these evoked-ATP release studies, an increase in extracellular ATP was estimated at about 1 μM; therefore, we expect that the spontaneous ATP release observed in this study potentially leads to similar effects on neurons. Moreover, it is also plausible that the spontaneously released ATP modulates not only the neuron activity but also the microglial surveillance or the blood flow control, which are associated with purinergic signaling (Császár et al., 2022; Haynes et al., 2006). Besides, as the loss of ATP release from astrocytes is related to psychiatric symptoms (Cao et al., 2013; Jun et al., 2018; Wang et al., 2021) and pathological conditions promote hyperactive extracellular ATP signaling (Delekate et al., 2014; Illes et al., 2019; Wu et al., 2022), future studies revealing how the spontaneous purinergic signaling of astrocytes is altered in pathological conditions will provide further insights into the roles of astrocytes both in physiological and pathophysiological conditions.

4.6 | Significance

The results presented in this study indicate that astrocytes spontaneously release ATP through multiple mechanisms, mainly in non-vesicular and Ca^{2+}-independent manners, which potentially coordinate hundreds of synapses at once. Our study, thus, provides three insights into astrocyte-neuron interaction mediated by gliotransmitter release: first, contrary to the classical regard for astrocytes as a passive element in the brain, astrocytes can provoke active communications independently of neuronal activity; second, our findings further strengthen the concept that neighboring synapses form functional islands regulated by purinergic signaling deriving from astrocytes; third, although Ca^{2+} activity is considered vital for astrocyte function, Ca^{2+}-independent processes may also play crucial roles in the gliotransmitter release.

4.7 | Limitations of the study

The present study has disclosed the spontaneous and localized release of ATP from astrocytes in culture and brain tissue, where we explored the mechanisms of this release, especially in slice preparation. Anesthetized mice, where neuronal inputs are depressed, also exhibit transient ATP release, however, its detailed mechanisms need to be thoroughly examined in vivo. Besides, while our work sheds light on spontaneously derived-ATP signaling in the cortex, further studies exploring other gliotransmitter dynamics in various brain regions are awaited to fully understand astrocyte-mediated active communications.

AUTHOR CONTRIBUTIONS

Conceptualization: Yoshiki Hatashita, Hirotaka Fujita, and Takafumi Inoue. *Investigation*: Yoshiki Hatashita and Zhaofa Wu. *Visualization*: Yoshiki Hatashita and Zhaofa Wu. *Formal analysis*: Yoshiki Hatashita, Zhaofa Wu, and Manabu Tanifuji. *Resources*: Zhaofa Wu, Takuma Kumamoto, Jean Livet, Yulong Li. *Supervision*: Takafumi Inoue. *Writing-original draft*: Yoshiki Hatashita and Takafumi Inoue. *Writing-review & editing*: all authors.

ACKNOWLEDGMENTS

This work was supported by Waseda University Grants for Special Research Projects (2019C-715, 2020C-778, 2021C-733, 2022C-629) to Takafumi Inoue; IHU FOReSIGHT (ANR-18-IAHU-01) to Jean Livet. Yoshiki Hatashita is supported by the Grant for Doctor 21 from the Yoshida Scholarship Foundation. Zhaofa Wu is supported in part by the Postdoctoral Fellowship of Peking-Tsinghua Center for Life Sciences.

CONFLICT OF INTEREST STATEMENT

The authors declare that there is no conflict of interest.

DATA AVAILABILITY STATEMENT

The data supporting the findings of this study are available from the corresponding author upon reasonable request.

ORCID

Yoshiki Hatashita https://orcid.org/0000-0002-5108-5986
Zhaofa Wu https://orcid.org/0000-0003-2027-5194
Jean Livet https://orcid.org/0000-0003-3079-4908
Takafumi Inoue https://orcid.org/0000-0002-2728-0060

REFERENCES

Agarwal, A., Wu, P.-H., Hughes, E. G., Fukaya, M., Tischfield, M. A., Langseth, A. J., Wirtz, D., & Bergles, D. E. (2017). Transient opening of the mitochondrial permeability transition pore induces microdomain calcium transients in astrocyte processes. *Neuron*, *93*, 587–605.e7.

Agulhon, C., Sun, M.-Y., Murphy, T., Myers, T., Lauderdale, K., & Fiacco, T. A. (2012). Calcium signaling and gliotransmission in normal vs. reactive astrocytes. *Frontiers in Pharmacology*, *3*, 139.

Araque, A., Carmignoto, G., Haydon, P. G., Oliet, S. H. R., Robitaille, R., & Volterra, A. (2014). Gliotransmitters travel in time and space. *Neuron*, *81*, 728–739.

Arizono, M., Inavalli, V. V. G. K., Panatier, A., Pfeiffer, T., Angibaud, J., Levet, F., Ter Veer, M. J. T., Stobart, J., Bellocchio, L., Mikoshiba, K., Marsicano, G., Weber, B., Oliet, S. H. R., & Nägerl, U. V. (2020). Structural basis of astrocytic Ca^{2+} signals at tripartite synapses. *Nature Communications*, *11*, 1906.

Aten, S., Kiyoshi, C. M., Arzola, E. P., Patterson, J. A., Taylor, A. T., Du, Y., Guiher, A. M., Philip, M., Camacho, E. G., Mediratta, D., Collins, K., Boni, K., Garcia, S. A., Kumar, R., Drake, A. N., Hegazi, A., Trank, L., Benson, E., Kidd, G., … Zhou, M. (2022). Ultrastructural view of astrocyte arborization, astrocyte-astrocyte and astrocyte-synapse contacts, intracellular vesicle-like structures, and mitochondrial network. *Progress in Neurobiology*, *213*, 102264.

Bazargani, N., & Attwell, D. (2016). Astrocyte calcium signaling: The third wave. *Nature Neuroscience*, *19*, 182–189.

Berg-Johnsen, J., Paulsen, R. E., Fonnum, F., & Langmoen, I. A. (1993). Changes in evoked potentials and amino acid content during fluorocitrate action studied in rat hippocampal cortex. *Experimental Brain Research*, *96*(2), 241–246.

Bindocci, E., Savtchouk, I., Liaudet, N., Becker, D., Carriero, G., & Volterra, A. (2017). Three-dimensional Ca^{2+} imaging advances understanding of astrocyte biology. *Science*, *356*, eaai8185.

Bonansco, C., Couve, A., Perea, G., Ferradas, C. Á., Roncagliolo, M., & Fuenzalida, M. (2011). Glutamate released spontaneously from astrocytes sets the threshold for synaptic plasticity: Setting neurotransmitter release probability by astrocytes. *European Journal of Neuroscience*, *33*, 1483–1492.

Cao, X., Li, L.-P., Wang, Q., Wu, Q., Hu, H.-H., Zhang, M., Fang, Y.-Y., Zhang, J., Li, S.-J., Xiong, W.-C., Yan, H.-C., Gao, Y.-B., Liu, J.-H., Li, X.-W., Sun, L.-R., Zeng, Y.-N., Zhu, X.-H., & Gao, T.-M. (2013). Astrocyte-derived ATP modulates depressive-like behaviors. *Nature Medicine*, *19*, 773–777.

Chai, H., Diaz-Castro, B., Shigetomi, E., Monte, E., Octeau, J. C., Yu, X., Cohn, W., Rajendran, P. S., Vondriska, T. M., Whitelegge, J. P., Coppola, G., & Khakh, B. S. (2017). Neural circuit-specialized astrocytes: Transcriptomic, proteomic, morphological, and functional evidence. *Neuron*, *95*, 531–549.e9.

Chever, O., Lee, C.-Y., & Rouach, N. (2014). Astroglial Connexin43 Hemichannels tune basal excitatory synaptic transmission. *The Journal of Neuroscience*, *34*, 11228–11232.

Chi, S., Cui, Y., Wang, H., Jiang, J., Zhang, T., Sun, S., Zhou, Z., Zhong, Y., & Xiao, B. (2022). Astrocytic Piezo1-mediated mechanotransduction determines adult neurogenesis and cognitive functions. *Neuron*, *110*, 2984–2999.e8.

Conley, J. M., Radhakrishnan, S., Valentino, S. A., & Tantama, M. (2017). Imaging extracellular ATP with a genetically-encoded, ratiometric fluorescent sensor. *PLoS One*, *12*, e0187481.

Covelo, A., & Araque, A. (2018). Neuronal activity determines distinct gliotransmitter release from a single astrocyte. *eLife*, *7*, e32237.

Császár, E., Lénárt, N., Cserép, C., Környei, Z., Fekete, R., Pósfai, B., Balázsfi, D., Hangya, B., Schwarcz, A. D., Szabadits, E., Szöllősi, D., Szigeti, K., Máthé, D., West, B. L., Sviatkó, K., Brás, A. R., Mariani, J.-C., Kliewer, A., Lenkei, Z., … Dénes, Á. (2022). Microglia modulate blood flow, neurovascular coupling, and hypoperfusion via purinergic actions. *Journal of Experimental Medicine*, *219*, e20211071.

Delekate, A., Füchtemeier, M., Schumacher, T., Ulbrich, C., Foddis, M., & Petzold, G. C. (2014). Metabotropic P2Y1 receptor signalling mediates astrocytic hyperactivity in vivo in an Alzheimer's disease mouse model. *Nature Communications*, *5*, 5422.

Fiacco, T. A., & McCarthy, K. D. (2018). Multiple lines of evidence indicate that Gliotransmission does not occur under physiological conditions. *The Journal of Neuroscience*, *38*, 3–13.

Fixt, E., & Hodges, J. L. (1951). Discriminatory analysis. Nonparametric discrimination: Consistency properties. US Air Force School of Aviation Medicine Technical Report 4:11.

Fujii, Y., Maekawa, S., & Morita, M. (2017). Astrocyte calcium waves propagate proximally by gap junction and distally by extracellular diffusion of ATP released from volume-regulated anion channels. *Scientific Reports*, *7*, 13115.

Giaume, C., Leybaert, L., C. Naus, C., & C. Sáez, J. (2013). Connexin and pannexin hemichannels in brain glial cells: Properties, pharmacology, and roles. *Frontiers in Pharmacology*, *4*, 88.

Guerra-Gomes, S., Sousa, N., Pinto, L., & Oliveira, J. F. (2018). Functional roles of astrocyte calcium elevations: From synapses to behavior. *Frontiers in Cellular Neuroscience*, *11*, 427.

Guthrie, P. B., Knappenberger, J., Segal, M., Bennett, M. V. L., Charles, A. C., & Kater, S. B. (1999). ATP released from astrocytes mediates glial calcium waves. *The Journal of Neuroscience*, *19*, 520–528.

Halassa, M. M., Fellin, T., Takano, H., Dong, J.-H., & Haydon, P. G. (2007). Synaptic Islands defined by the territory of a single astrocyte. *The Journal of Neuroscience*, *27*, 6473–6477.

Halassa, M. M., Florian, C., Fellin, T., Munoz, J. R., Lee, S.-Y., Abel, T., Haydon, P. G., & Frank, M. G. (2009). Astrocytic modulation of sleep homeostasis and cognitive consequences of sleep loss. *Neuron*, *61*, 213–219.

Halassa, M. M., & Haydon, P. G. (2010). Integrated brain circuits: Astrocytic networks modulate neuronal activity and behavior. *Annual Review of Physiology*, *72*, 335–355.

Harris, C. R., Millman, K. J., van der Walt, S. J., Gommers, R., Virtanen, P., Cournapeau, D., Wieser, E., Taylor, J., Berg, S., Smith, N. J., Kern, R., Picus, M., Hoyer, S., van Kerkwijk, M. H., Brett, M., Haldane, A., Del Río, J. F., Wiebe, M., Peterson, P., … Oliphant, T. E. (2020). Array programming with NumPy. *Nature*, *585*, 357–362.

Haustein, M. D., Kracun, S., Lu, X.-H., Shih, T., Jackson-Weaver, O., Tong, X., Xu, J., Yang, X. W., O'Dell, T. J., Marvin, J. S., Ellisman, M. H., Bushong, E. A., Looger, L. L., & Khakh, B. S. (2014). Conditions and constraints for astrocyte calcium signaling in the hippocampal mossy fiber pathway. *Neuron*, *82*, 413–429.

Haynes, S. E., Hollopeter, G., Yang, G., Kurpius, D., Dailey, M. E., Gan, W.-B., & Julius, D. (2006). The $P2Y_{12}$ receptor regulates microglial activation by extracellular nucleotides. *Nature Neuroscience*, *9*, 1512–1519.

Henneberger, C., Papouin, T., Oliet, S. H. R., & Rusakov, D. A. (2010). Long-term potentiation depends on release of d-serine from astrocytes. *Nature*, *463*, 232–236.

Illes, P., Burnstock, G., & Tang, Y. (2019). Astroglia-derived ATP modulates CNS neuronal circuits. *Trends in Neurosciences*, *42*, 885–898.

Inoue, T. (2018). TI Workbench, an integrated software package for electrophysiology and imaging. *Microscopy*, *67*, 129–143.

Iwai, Y., Ozawa, K., Yahagi, K., Mishima, T., Akther, S., Vo, C. T., Lee, A. B., Tanaka, M., Itohara, S., & Hirase, H. (2021). Transient astrocytic Gq signaling underlies remote memory enhancement. *Frontiers in Neural Circuits*, *15*, 658343.

Jun, M., Xiaolong, Q., Chaojuan, Y., Ruiyuan, P., Shukun, W., Junbing, W., Li, H., Hong, C., Jinbo, C., Rong, W., Yajin, L., Lanqun, M., Fengchao, W., Zhiying, W., Jianxiong, A., Yun, W., Xia, Z., Chen, Z., & Zengqiang, Y. (2018). Calhm2 governs astrocytic ATP releasing in the development of depression-like behaviors. *Molecular Psychiatry*, *23*, 883–891.

Kamatsuka, Y., Fukagawa, M., Furuta, T., Ohishi, A., Nishida, K., & Nagasawa, K. (2014). Astrocytes, but not neurons, exhibit constitutive activation of P2X7 receptors in mouse acute cortical slices under non-stimulated resting conditions. *Biological & Pharmaceutical Bulletin*, *37*, 1958–1962.

Khakh, B. S., & North, R. A. (2012). Neuromodulation by extracellular ATP and P2X receptors in the CNS. *Neuron*, *76*, 51–69.

Kikuchi, T., Gonzalez-Soriano, J., Kastanauskaite, A., Benavides-Piccione, R., Merchan-Perez, A., DeFelipe, J., & Blazquez-Llorca, L. (2020). Volume electron microscopy study of the relationship between synapses and astrocytes in the developing rat somatosensory cortex. *Cerebral Cortex*, *30*, 3800–3819.

Koizumi, S., Fujishita, K., Tsuda, M., Shigemoto-Mogami, Y., & Inoue, K. (2003). Dynamic inhibition of excitatory synaptic transmission by astrocyte-derived ATP in hippocampal cultures. *Proceedings of the National Academy of Sciences of the United States of America*, *100*, 11023–11028.

Kumamoto, T., Maurinot, F., Barry-Martinet, R., Vaslin, C., Vandormael-Pournin, S., Le, M., Lerat, M., Niculescu, D., Cohen-Tannoudji, M., Rebsam, A., Loulier, K., Nedelec, S., Tozer, S., & Livet, J. (2020). Direct readout of neural stem cell Transgenesis with an integration-coupled gene expression switch. *Neuron*, *107*, 617–630.e6.

Lalo, U., Palygin, O., Rasooli-Nejad, S., Andrew, J., Haydon, P. G., & Pankratov, Y. (2014). Exocytosis of ATP from astrocytes modulates phasic and tonic inhibition in the neocortex. *PLoS Biology*, *12*, e1001747.

Li, B., Chavarha, M., Kobayashi, Y., Yoshinaga, S., Nakajima, K., Lin, M. Z., & Inoue, T. (2020). Two-photon voltage imaging of spontaneous activity from multiple neurons reveals network activity in brain tissue. *iScience*, *23*, 101363.

Li, D., Hérault, K., Zylbersztejn, K., Lauterbach, M. A., Guillon, M., Oheim, M., & Ropert, N. (2015). Astrocyte VAMP3 vesicles undergo Ca^{2+}-independent cycling and modulate glutamate transporter trafficking: Trafficking of astrocyte VAMP3 vesicles. *The Journal of Physiology*, *593*, 2807–2832.

Li, X., Li, Y., Zhou, Y., Wu, J., Zhao, Z., Fan, J., Deng, F., Wu, Z., Xiao, G., He, J., Zhang, Y., Zhang, G., Hu, X., Chen, X., Zhang, Y., Qiao, H., Xie, H., Li, Y., Wang, H., … Dai, Q. (2022). Real-time denoising enables high-sensitivity fluorescence time-lapse imaging beyond the shot-noise limit. *Nature Biotechnology*, *41*, 282–292.

Liu, H.-T., Sabirov, R. Z., & Okada, Y. (2008). Oxygen-glucose deprivation induces ATP release via maxi-anion channels in astrocytes. *Purinergic Signalling*, *4*, 147–154.

Lobas, M. A., Tao, R., Nagai, J., Kronschläger, M. T., Borden, P. M., Marvin, J. S., Looger, L. L., & Khakh, B. S. (2019). A genetically encoded single-wavelength sensor for imaging cytosolic and cell surface ATP. *Nature Communications*, *10*, 711.

McInnes, L., Healy, J., & Melville, J. (2018). UMAP: Uniform manifold approximation and projection for dimension reduction. arXiv [Internet]. https://arxiv.org/abs/1802.03426

McKinney, W. (2010). Data structures for statistical computing in python. In *Proceedings of the 9th Python in Science Conference* (Vol. 445, pp. 51–56). SciPy. https://doi.org/10.25080/Majora-92bf1922-00a

Mederos, S., Hernández-Vivanco, A., Ramírez-Franco, J., Martín-Fernández, M., Navarrete, M., Yang, A., Boyden, E. S., & Perea, G. (2019). Melanopsin for precise optogenetic activation of astrocyte-neuron networks. *Glia*, *67*, 915–934.

Morel, L., Men, Y., Chiang, M. S. R., Tian, Y., Jin, S., Yelick, J., Higashimori, H., & Yang, Y. (2019). Intracortical astrocyte subpopulations defined by astrocyte reporter mice in the adult brain. *Glia*, *67*, 171–181.

Motohashi, K. (2015). A simple and efficient seamless DNA cloning method using SLiCE from Escherichia coli laboratory strains and its application to SLiP site-directed mutagenesis. *BMC Biotechnology*, *15*, 47.

Panatier, A., Vallée, J., Haber, M., Murai, K. K., Lacaille, J.-C., & Robitaille, R. (2011). Astrocytes are endogenous regulators of basal transmission at central synapses. *Cell*, *146*, 785–798.

Paparrizos, J., & Gravano, L. (2015). k-shape: Efficient and accurate clustering of time series. In *Proceedings of the 2015 ACM SIGMOD international conference on Management of Data* (pp. 1855–1870). ACM. https://doi.org/10.1145/2723372.2737793

Paulsen, R. E., Contestabile, A., Villani, L., & Fonnum, F. (1987). An In vivo model for studying function of brain tissue temporarily devoid of glial cell metabolism: The use of Fluorocitrate. *Journal of Neurochemistry*, *48*, 1377–1385.

Pedregosa, F., Varoquaux, G., Gramfort, A., Michel, V., Thirion, B., Grisel, O., Blondel, M., Prettenhofer, P., Weiss, R., Dubourg, V., Vanderplas, J., Passos, A., & Cournapeau, D. (2011). Scikit-learn: Machine learning in python. *Journal of Machine Learning Research*, *12*, 2825–2830.

Perea, G. (2005). Properties of synaptically evoked astrocyte calcium signal reveal synaptic information processing by astrocytes. *The Journal of Neuroscience*, *25*, 2192–2203.

Perea, G., & Araque, A. (2007). Astrocytes potentiate transmitter release at single hippocampal synapses. *Science*, *317*, 1083–1086.

Prochnow, N., Abdulazim, A., Kurtenbach, S., Wildförster, V., Dvoriantchikova, G., Hanske, J., Petrasch-Parwez, E., Shestopalov, V. I., Dermietzel, R., Manahan-Vaughan, D., & Zoidl, G. (2012). Pannexin1 stabilizes synaptic plasticity and is needed for learning. *PLoS One*, *7*, e51767.

Rungta, R. L., Bernier, L.-P., Dissing-Olesen, L., Groten, C. J., LeDue, J. M., Ko, R., Drissler, S., & MacVicar, B. A. (2016). Ca^{2+} transients in astrocyte fine processes occur via Ca^{2+} influx in the adult mouse hippocampus: Ca^{2+} transients in astrocyte fine processes. *Glia*, *64*, 2093–2103.

Sahlender, D. A., Savtchouk, I., & Volterra, A. (2014). What do we know about gliotransmitter release from astrocytes? *Philosophical Transactions of the Royal Society B*, *369*, 20130592.

Savtchouk, I., & Volterra, A. (2018). Gliotransmission: Beyond black-and-white. *The Journal of Neuroscience*, *38*, 14–25.

Schmidt, E., & Oheim, M. (2020). Infrared excitation induces heating and calcium microdomain hyperactivity in cortical astrocytes. *Biophysical Journal*, *119*, 2153–2165.

Schneider, C. A., Rasband, W. S., & Eliceiri, K. W. (2012). NIH image to ImageJ: 25 years of image analysis. *Nature Methods*, *9*, 671–675.

Semyanov, A. (2019). Spatiotemporal pattern of calcium activity in astrocytic network. *Cell Calcium*, *78*, 15–25.

Shen, W., Nikolic, L., Meunier, C., Pfrieger, F., & Audinat, E. (2017). An autocrine purinergic signaling controls astrocyte-induced neuronal excitation. *Scientific Reports*, *7*, 11280.

Shigetomi, E., Patel, S., & Khakh, B. S. (2016). Probing the complexities of astrocyte calcium signaling. *Trends in Cell Biology*, *26*, 300–312.

Stehberg, J., Moraga-Amaro, R., Salazar, C., Becerra, A., Echeverría, C., Orellana, J. A., Bultynck, G., Ponsaerts, R., Leybaert, L., Simon, F., Sáez, J. C., & Retamal, M. A. (2012). Release of gliotransmitters through astroglial connexin 43 hemichannels is necessary for fear memory consolidation in the basolateral amygdala. *The FASEB Journal*, *26*, 3649–3657.

Stone, E. A., Sessler, F. M., & Weimin, L. (1990). Glial localization of adenylate-cyclase-coupled β-adrenoreceptors in rat forebrain slices. *Brain Research*, *530*, 295–300.

Suadicani, S. O., Iglesias, R., Wang, J., Dahl, G., Spray, D. C., & Scemes, E. (2012). ATP signaling is deficient in cultured pannexin1-null mouse astrocytes. *Glia*, *60*, 1106–1116.

Takata, N., & Hirase, H. (2008). Cortical layer 1 and layer 2/3 astrocytes exhibit distinct calcium dynamics In vivo. *PLoS One*, *3*, e2525.

Tan, Z., Liu, Y., Xi, W., Lou, H., Zhu, L., Guo, Z., Mei, L., & Duan, S. (2017). Glia-derived ATP inversely regulates excitability of pyramidal and CCK-positive neurons. *Nature Communications*, *8*, 13772.

Taruno, A. (2018). ATP release channels. *International Journal of Molecular Sciences*, *19*, 808.

Thévenaz, P., Ruttimann, U. E., & Unser, M. (1998). A pyramid approach to subpixel registration based on intensity. *IEEE Trans on Image Process*, *7*, 27–41.

Virtanen, P., Gommers, R., Oliphant, T. E., Haberland, M., Reddy, T., Cournapeau, D., Burovski, E., Peterson, P., Weckesser, W., Bright, J., van der Walt, S. J., Brett, M., Wilson, J., Millman, K. J., Mayorov, N., Nelson, A. R. J., Jones, E., Kern, R., Larson, E., … SciPy 1.0 Contributors. (2020). SciPy 1.0: Fundamental algorithms for scientific computing in Python. *Nature Methods*, *17*, 261–272.

Vitiello, L., Gorini, S., Rosano, G., & la Sala, A. (2012). Immunoregulation through extracellular nucleotides. *Blood*, *120*, 511–518.

Wang, Q., Kong, Y., Wu, D.-Y., Liu, J.-H., Jie, W., You, Q.-L., Huang, L., Hu, J., Chu, H.-D., Gao, F., Hu, N.-Y., Luo, Z.-C., Li, X.-W., Li, S.-J., Wu, Z.-F., Li, Y.-L., Yang, J.-M., & Gao, T.-M. (2021). Impaired calcium signaling in astrocytes modulates autism spectrum disorder-like behaviors in mice. *Nature Communications*, *12*, 3321.

Wang, Y., DelRosso, N. V., Vaidyanathan, T. V., Cahill, M. K., Reitman, M. E., Pittolo, S., Mi, X., Yu, G., & Poskanzer, K. E. (2019). Accurate quantification of astrocyte and neurotransmitter fluorescence dynamics for single-cell and population-level physiology. *Nature Neuroscience*, *22*, 1936–1944.

Ward, J. H. (1963). Hierarchical grouping to optimize an objective function. *Journal of the American Statistical Association*, *58*, 236–244.

Wu, J., Abdelfattah, A. S., Miraucourt, L. S., Kutsarova, E., Ruangkittisakul, A., Zhou, H., Ballanyi, K., Wicks, G., Drobizhev, M., Rebane, A., Ruthazer, E. S., & Campbell, R. E. (2014). A long stokes shift red fluorescent Ca^{2+} indicator protein for two-photon and ratiometric imaging. *Nature Communications*, *5*, 5262.

Wu, Y.-W., Gordleeva, S., Tang, X., Shih, P.-Y., Dembitskaya, Y., & Semyanov, A. (2019). Morphological profile determines the frequency of spontaneous calcium events in astrocytic processes. *Glia*, *67*, 246–262.

Wu, Z., He, K., Chen, Y., Li, H., Pan, S., Li, B., Liu, T., Xi, F., Deng, F., Wang, H., Du, J., Jing, M., & Li, Y. (2022). A sensitive GRAB sensor for detecting extracellular ATP in vitro and in vivo. *Neuron*, *110*, 770–782.e5.

Wu, Z., & Li, Y. (2020). New frontiers in probing the dynamics of purinergic transmitters in vivo. *Neuroscience Research*, *152*, 35–43.

Zhang, J., Wang, H., Ye, C., Ge, W., Chen, Y., Jiang, Z., Wu, C., Poo, M., & Duan, S. (2003). ATP released by astrocytes mediates glutamatergic activity-dependent heterosynaptic suppression. *Neuron*, *40*, 971–982.

Zhao, Y.-J., Yu, T.-T., Zhang, C., Li, Z., Luo, Q.-M., Xu, T.-H., & Zhu, D. (2018). Skull optical clearing window for in vivo imaging of the mouse cortex at synaptic resolution. *Light: Science & Applications*, *7*, 17153.

SUPPORTING INFORMATION

Additional supporting information can be found online in the Supporting Information section at the end of this article.

How to cite this article: Hatashita, Y., Wu, Z., Fujita, H., Kumamoto, T., Livet, J., Li, Y., Tanifuji, M., & Inoue, T. (2023). Spontaneous and multifaceted ATP release from astrocytes at the scale of hundreds of synapses. *Glia*, *71*(9), 2250–2265. https://doi.org/10.1002/glia.24392